

## Recycled volatiles determine fertility of porphyry deposits in collisional settings

BO XU<sup>1,2,\*</sup>, ZENG-QIAN HOU<sup>3</sup>, WILLIAM L. GRIFFIN<sup>2</sup>, YONGJUN LU<sup>4,5</sup>, ELENA BELOUSOVA<sup>2</sup>,  
JI-FENG XU<sup>1</sup>, AND SUZANNE Y. O'REILLY<sup>2</sup>

<sup>1</sup>State Key Laboratory of Geological Processes and Mineral Resources, China University of Geosciences, Beijing 100083, China

<sup>2</sup>ARC Centre of Excellence for Core to Crust Fluid Systems (CCFS) and GEMOC, Macquarie University, New South Wales 2109, Australia

<sup>3</sup>Chinese Academy of Geological Sciences, Beijing 100037, China

<sup>4</sup>Geological Survey of Western Australia, 100 Plain Street, East Perth, Western Australia 6004, Australia

<sup>5</sup>Centre for Exploration Targeting and CCFS, School of Earth Sciences, The University of Western Australia, Crawley, Western Australia 6009, Australia

### ABSTRACT

An intensive study of the geochemical characteristics (including the volatile elements Cl and S) of apatite associated with porphyry deposits was undertaken to address the debate about the crust- or mantle-derivation of their copper and gold and to better understand the controls on the transport of metals in magmatic fluids in post-subduction settings. New geochemical data on apatite reveal parameters to discriminate mineralized porphyry systems across Iran and western China (Tibet and Yunnan), from coeval barren localities across this post-subduction metallogenic belt. Apatites in *fertile* porphyries have higher Cl and S concentrations (reflecting water-rich crystallization conditions) than those from coeval *barren* ones. Our new isotopic data also indicate these volatiles are likely derived from pre-enriched sub-continental lithospheric mantle, metasomatized by previous oceanic subduction. This study demonstrates that refertilization of suprasubduction lithospheric mantle during previous collision events is a prerequisite for forming post-subduction fertile porphyries, providing an evidence-based alternative to current ore-enrichment models.

**Keywords:** Collisional settings, in situ isotope, deposits, Tibet

### INTRODUCTION

The Earth's mantle and crust contain little copper and gold, and thus the concentration of these elements to form ore deposits requires an explanation of their origin (crust or mantle) and the processes required (Sillitoe 2010). Volatiles such as chlorine, sulfur, and water are of paramount importance for the transport and deposition of copper and gold (Griffin et al. 2013; Tassara et al. 2017) and carry the keys to examining this problem. The Tethyan metallogenic belt, extending from Europe through Iran to Tibet, is one of the world's major metal-producing belts. It contains many post-collisional porphyry deposits and is an ideal natural laboratory to examine the origins of important volatile components and the related mechanisms for post-subduction porphyry mineralization.

Volatiles are difficult to study in whole-rock samples, owing to alteration and weathering. However, apatite concentrates volatiles (e.g., chlorine and sulfur) that are ubiquitous in the lithospheric mantle (O'Reilly and Griffin 2000) and crust (Bruand et al. 2019) and especially apatite crystallizes early in porphyry systems (Mao et al. 2016). Apatite, therefore, can record a more complete history of the evolution of volatiles in these magmas (Chelle-Michou et al. 2017).

In this study, we use in situ major- and trace-element geochemistry and Sr isotopes of magmatic apatite in porphyries from 12 porphyry Cu±Au±Mo deposits and 7 barren suites within the Tethyan metallogenic belt. The sample suite includes the largest porphyry deposits in each mineralized domain. These data reveal

(1) anomalous enrichment of chlorine and sulfur in ore-forming magmas, and (2) a mantle isotopic signature in fertile suites.

### SAMPLES


Fifty samples from 12 fertile porphyry deposits and 7 barren locations in four major post-subduction arcs (Fig. 1) have been analyzed, including the two largest porphyry systems in Iran, the Sarcheshmeh and Sungun deposits in the Kerman and Arasbaran porphyry copper belt; the deposits in the Gangdese belt, southern Tibet; and the porphyry systems in the Sanjiang orogen in southeast Tibet (Online Material<sup>1</sup> Fig. OM1). All samples represent post-collisional magmatism following cessation of active subduction. The description of the deposits and the barren plutons is given in the Online Material<sup>1</sup>. The apatite samples were collected from fresh magmatic apatite, without zoning and extensive resorption texture from BSE images (Online Material<sup>1</sup>). To yield robust apatite data, especially for the S, Cl, and isotopic analysis, we carried out 244 major-element and 562 trace-element analysis on seven different apatite standards and synthetic materials, including Durango (Mexico), Mad-blue, Mad-green (Madagascar), Moy (Myanmar), Mud Tank (Australia), and Kovdor and Sly (Russia). Rb-Sr isotopes in apatites with different Sr concentrations were measured by the solution method and then used as monitoring standards. The description of standards and analytical methods is given in the Online Material<sup>1</sup>.

### RESULTS

#### Chlorine, sulfur, and rare-earth elements

The chlorine contents of apatite from the ore-forming porphyries are generally higher than those of apatite from the barren

\* E-mail: xubo@outlook.com.cn

 Open access: Article available to all readers online.

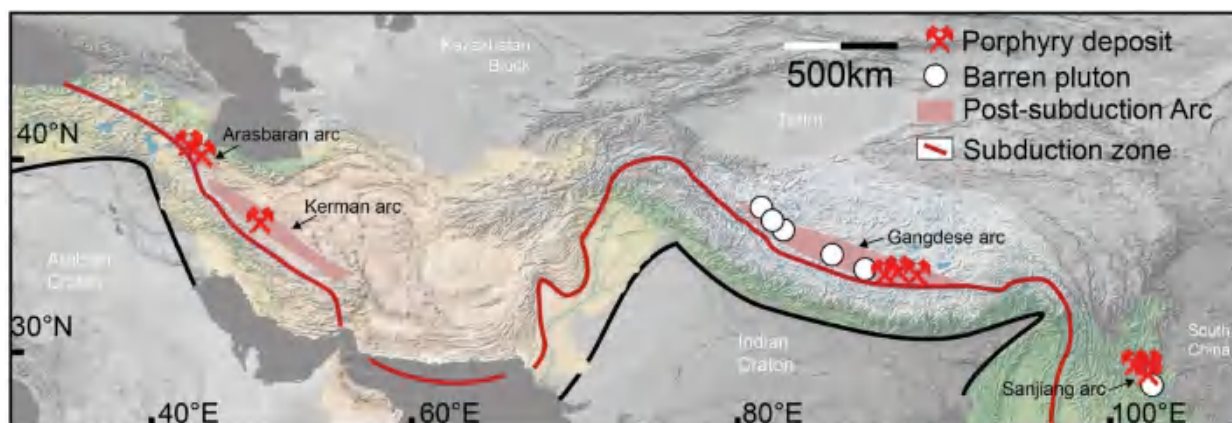


**FIGURE 1.** Global relief map showing the distribution of the fertile and barren magmatic suites investigated in this study (listed in Table 1). The names of the fertile and barren suites used in this study are labeled on the map.

plutons (fertile suites: 0.08–0.34 wt%; median 0.13 wt%, average 0.17 wt%; barren suites: 0–0.34 wt%; median 0.03 wt%, average 0.04 wt%). For example, apatite in the Sarcheshmeh and Sungun porphyry Cu deposits contains 0.89 to 1.36 wt% and 0.42 to 1.64 wt% Cl, respectively; comparative values are 0.12 to 0.58 wt% Cl in the Qulong porphyry Cu-Mo deposit, ~0.06 to 0.23 wt% Cl in the Jiama porphyry-skarn Cu-Mo-Au deposit, 0.02 to 0.12 wt% Cl in the Beiya porphyry-skarn Cu-Mo-Au deposit, and 0.12 to 0.41 wt% Cl in the Machangqing porphyry deposit (Fig. 2a; Table 1). In contrast, 95% apatites from barren suites contain <0.1 wt% Cl. Sulfur enters the apatite structure by complex substitutions including  $\text{Na}^+ + \text{S}^{6+} = \text{Ca}^{2+} + \text{P}^{5+}$  and  $\text{S}^{6+} + \text{Si}^{4+} = 2\text{P}^{5+}$  (Sha and Chappell 1999). The  $\text{SO}_3$  contents in apatite from the fertile suites (<0.96 wt%; median 0.15 wt%, average 0.19 wt%) are higher than those in apatite from the barren suites (<0.75 wt%; median 0.07 wt%, average 0.10 wt%; Fig. 2a). REEs and Y are incorporated into the apatite structure via coupled substitutions (Hughes and Rakovan 2015):  $\text{Na}^+ + (\text{Y} + \text{REE})^{3+} = 2\text{Ca}^{2+}$  and  $\text{Si}^{4+} + (\text{Y} + \text{REE})^{3+} = \text{P}^{5+} + \text{Ca}^{2+}$ . Apatites in the mineralized samples have higher contents of REEs+Y (28–23 000 ppm; median 520 ppm, average: 6650 ppm) than those in the barren rocks (68–55 400 ppm; median 3230 ppm, average: 4110 ppm; Figs. 2b). The barren and fertile suites can also be distinguished on a series of trace-element plots involving  $(\text{Ce}/\text{Pb})_N$ ,  $(\text{La}/\text{Yb})_N$ , and  $(\text{V}/\text{Y})$  (Fig. 2b). In detail, apatites from most of the fertile-suite samples have higher  $(\text{La}/\text{Yb})_N$  (fertile suite: 2–206; median 67, average 73; barren suite: 0–155; median 18, average 23) and  $\text{V}/\text{Y}$  (fertile suite: <0.4; median 0.04, average 0.05; barren suite: 0–18.0; median 0.02, average 0.17). The trace-element patterns of apatite from both groups display smooth patterns with relative enrichments of LREEs relative to HREEs. All samples, except the Yao'an apatite, show negative Eu anomalies (Online Material<sup>1</sup> Fig. OM4).

#### In situ Sr isotope compositions of apatite

In situ Sr-isotope analyses (205 measurements) have been carried out on apatites from the fertile rocks including Sungun, Sarcheshmeh, Masjed Daghi, Zhunuo, Jiama, Qulong, Machangqing, and Yaoan porphyries, and on apatite grains within the barren Zhada, Nanmuqie, Renduoxiang, Wolong, and Songgui plutons. Apatite in the fertile suites show lower radiogenic

$^{87}\text{Sr}/^{86}\text{Sr}_i$  (0.704–0.709, median 0.706, average 0.706), whereas apatite from magmatic rocks of the barren suites has generally more radiogenic signatures ( $^{87}\text{Sr}/^{86}\text{Sr}_i = 0.705\text{--}0.712$ , median 0.708, average 0.708; Figs. 2d–2f).

## DISCUSSION

### Apatite trace elements reveal the hydrous source of porphyry systems

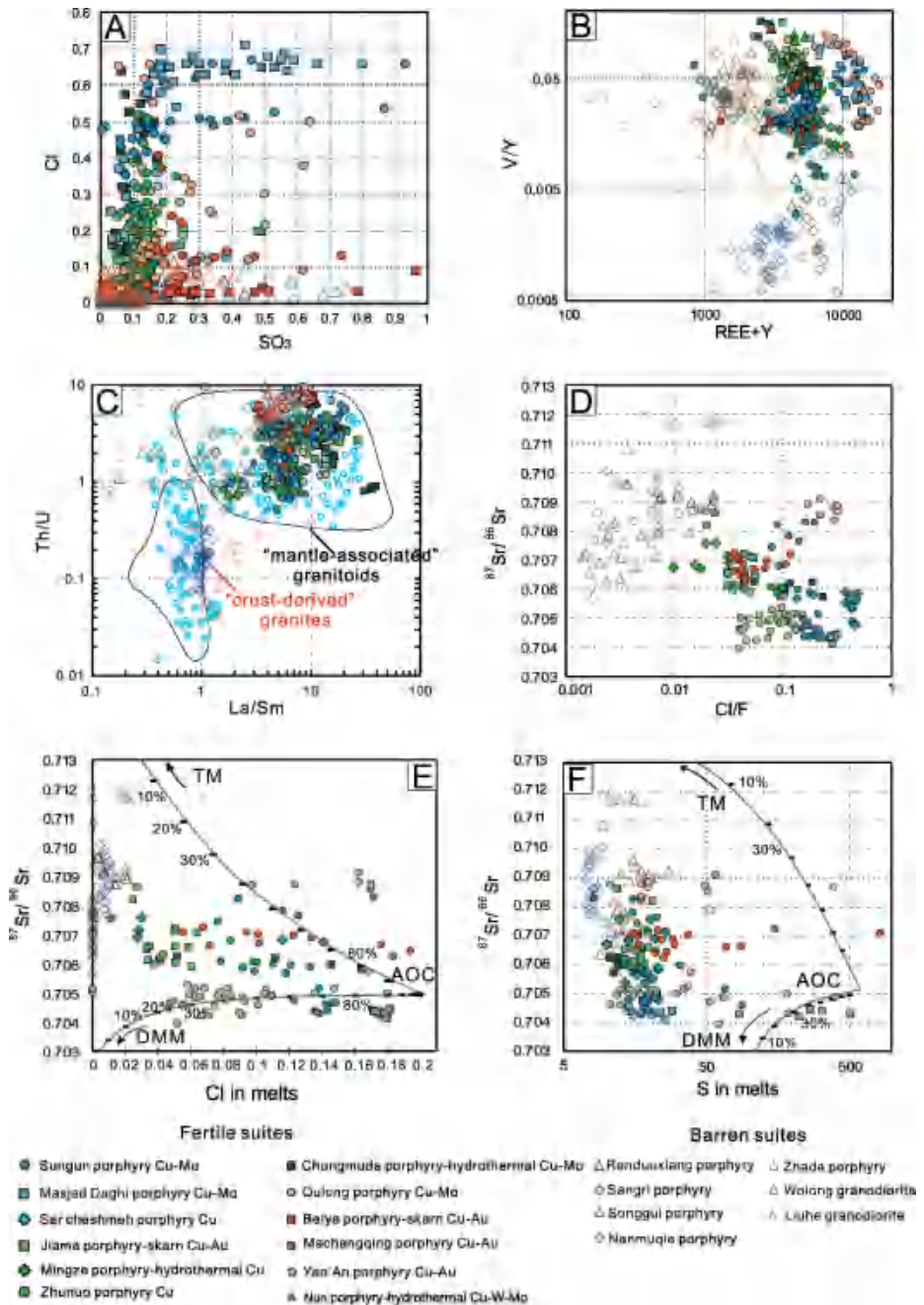
The euhedral apatites crystallized early, essentially coeval with, or before monazite and xenotime (Suzuki et al. 1992). Thus, euhedral apatite can be used as an indicator mineral to trace the composition of its parental melts. The role of high contents of magmatic water during the formation of porphyry-forming magmas has been widely discussed and is recognized as a key factor in the fertility of porphyry systems (Loucks 2014; Chiaradia 2014). Apatite in ore-forming magma has high  $\text{V}/\text{Y}$  (Fig. 2b). These higher V contents in the host magma indicates elevated contents of dissolved  $\text{H}_2\text{O}$  in the melt, which cause amphibole to advance in the crystallization sequence rather than titanomagnetite.  $\text{V}^{4+}$  partitions more strongly into magnetite than into amphibole [ $D_{\text{V}}^{\text{mag/melt}} > 130$ ;  $D_{\text{V}}^{\text{amp/melt}}: 6.34\text{--}10.64$  (La Tourrette et al. 1991; Nandedkar et al. 2016)]. Thus, at high contents of  $\text{H}_2\text{O}$  in the melt, amphibole will reach saturation before titanomagnetite, so that more V remains in the residual melt, while Y continues to be efficiently extracted from the melt into amphibole [the amphibole/melt partition coefficient for Y is around 2–6 in andesitic melts (Ewart and Griffin 1994)]. Therefore, apatite trace-element proxies for amphibole in the differentiation series are especially useful indicators of the hydration state of the melt as well as the pressure at which differentiation took place (Loucks 2014; Davidson et al. 2007). This is consistent with the geochemistry of such magmas, which are characterized by small negative Eu anomalies and high  $\text{V}/\text{Sc}$  and  $\text{Sr}/\text{Y}$  (Loucks 2014), reflecting early amphibole fractionation and suppression of plagioclase crystallization in hydrous melts (Davidson et al. 2007). Moreover, the rare-earth elements entrained by apatite are incompatible during magma evolution, and thus higher REEs in apatite also may suggest a hydrous magma. In detail, LREEs (e.g., La, Ce) are more compatible in hydrous melts than HREEs and Pb. As a consequence, hydrous melts usually contain higher LREE, which can be expressed by their  $(\text{Ce}/\text{Pb})_N$  ratio (Davidson et al. 2007).

► **FIGURE 2.** (a) Apatite Cl (wt%) vs.  $\text{SO}_3$  (wt%), (b) Apatite REE+Y (ppm) vs. V/Y plot, (c) Apatite Th/U vs. La/Sm, (d) Apatite Cl/F vs.  $^{87}\text{Sr}/^{86}\text{Sr}$  plot, (e) Apatite chlorine in melts vs.  $^{87}\text{Sr}/^{86}\text{Sr}$  plot, (f) Apatite sulfur in melts vs.  $^{87}\text{Sr}/^{86}\text{Sr}$  plot, showing that most fertile suites have high Cl, REE+Y content, and V/Y ratio; the fertile porphyries also have high chlorine and sulfur content in melts with less radiogenic  $^{87}\text{Sr}/^{86}\text{Sr}$ .

It is thus expected that the apatite in hydrous magmas should have higher  $(\text{Ce}/\text{Pb})_N$  than those in the relatively dry suites. Therefore, on plots of V/Y vs. REE+Y (Fig. 2b) and V/Y vs.  $(\text{Ce}/\text{Pb})_N$  and V/Y vs. REE+Y (Fig. DR3), the fertile suites mostly have higher ratios than barren suites, suggesting early amphibole fractionation in melts and reflecting the more hydrous nature of ore-forming magmas.

### Contrasting volatiles and Sr isotope compositions between fertile and barren melts in post-subduction settings

The composition of apatite can be used to calculate chlorine and sulfur concentrations in the parental melt, provided that the apatite and melt were in equilibrium, and that the experimental partition coefficients of these volatile components between the apatite and concomitant melt are known. The experimental and analytical results indicate that F, Cl, and OH in apatite can diffuse relatively rapidly along the crystallographic c-axis, and compositional gradients in these components can be observed if post-magmatic changes in temperature, pressure, and fluid or melt composition have occurred (Brenan 1993). Given these diffusion rates, the resistance of apatite to late re-equilibration may only be satisfied when the system cools rapidly ( $1^\circ\text{C}/100\text{ yr}$ ; Brenan et al. 1995), conditions which are likely in eruptive magmas or very shallowly emplaced melts (Piccoli and Candela 2002). However, these conditions may not easily be reached in porphyry magmas. We have analyzed the apatites from core to rim by electron microprobe analysis (EMPA), to quantify the degree of diffusion (Online Material<sup>1</sup> Fig. OM3). Cathodoluminescence and backscattered electron images were used to select analytical points. The Cl contents from core to rim



show little sign of zoning, indicating our samples were not affected by diffusion. Therefore, the chlorine contents of these apatites can be used to calculate the chlorine concentrations of the coexisting melt. Several previous experimental studies have determined the partitioning behavior of Cl and/or F in the apatite-fluids-silicate melt system at different shallow-crustal conditions (Parat and Holtz 2005). We have used the recently calibrated apatite/melt chlorine partitioning model of Li and Hermann (2017) based on experimental data from Webster et al. (2009) at 200 MPa and  $900^\circ\text{C}$ . We argue that the experimental conditions are reasonably close to those inferred at the time of apatite crystallization and

**TABLE 1.** Infertile and fertile magmatic suites used in this work

Sample	Deposit type	Apatite Cl (wt%)				Cl in melts (ppm)				Apatite SO <sub>3</sub> (wt%)				S in melts (ppm)			
		Max	Min	Avg	Med	Max	Min	Avg	Med	Max	Min	Avg	Med	Max	Min	Avg	Med
Masjed Daghi	Cu-Au	1.91	0.18	1.28	1.83	16529	1462	2695	1774	0.24	0.03	0.13	0.15	509.88	9.05	74.22	26.63
Sungun	Cu-Au	1.64	0.42	1.02	1.02	4475	1122	2400	2248	0.93	0.10	0.22	0.16	254.66	7.62	34.51	21.17
Sarcheshmeh	Cu-Au	1.36	0.89	1.17	1.18	382127	3825	32472	5424	0.20	0.09	0.15	0.16	27.93	13.51	20.52	20.64
Qulong	Cu-Mo	0.58	0.12	0.25	0.23	120095	474	4341	903	0.62	0.05	0.16	0.14	395.20	7.62	32.68	17.60
Zhunuao	Cu-Mo	0.52	0.22	0.29	0.27	1712	766	1025	972	0.23	0.06	0.12	0.12	32.96	11.16	17.13	15.85
Jiama	Cu-Au	0.23	0.06	0.14	0.14	8715	246	746	565	0.49	0.03	0.13	0.12	85.69	9.46	17.48	16.36
Chongmuda	Cu-Mo	0.64	0.14	0.38	0.40	3090	488	1264	1193	0.17	0.03	0.10	0.09	22.49	9.46	13.73	12.68
Nuri	Au-Cu	0.20	0.07	0.96	0.08	2169	0	347	0	0.28	0.12	0.22	0.23	45.61	16.46	32.91	32.03
Beiya	Au-Cu	0.12	0.02	0.04	0.04	920	356	653	653	0.96	0.01	0.30	0.26	197.38	7.91	52.68	36.27
Machangqing	Cu-Au	0.41	0.12	0.18	0.15	48098	0	5420	1015	0.74	0.01	0.25	0.19	151.05	15.35	38.18	25.22
Yaoan	Au	0.70	0.04	0.29	0.16	54810	206	4359	1625	0.64	0.05	0.22	0.16	443.21	10.68	54.88	20.84
Mingze	Au	0.12	0.03	0.08	0.07	3493	12	1003	302	0.19	0.04	0.10	0.08	25.55	7.62	12.99	11.80
Zhada	Barren	0.20	0.02	0.12	0.13	673	0	383	425	0.44	0.00	0.12	0.11	125.58	7.62	20.42	15.64
Renduoxiang	Barren	0.08	0.00	0.03	0.03	766	0	101	85	0.24	0.00	0.08	0.08	35.35	7.62	14.10	12.36
Nanmuqie	Barren	1.27	0.00	0.05	0.02	3329	7	142	72	0.14	0.00	0.01	0.01	18.58	7.15	8.49	8.12
Sangri	Barren	0.40	0.00	0.03	0.03	1127	0	103	104	0.59	0.00	0.08	0.09	27.23	7.62	13.21	13.51
Wolong	Barren	0.06	0.00	0.01	0.01	0	0	0	0	0.72	0.00	0.15	0.05	742.46	7.62	73.87	10.54
Liuhe	Barren	0.34	0.00	0.06	0.04	1309	187	565	389	0.52	0.00	0.09	0.05	203.77	7.62	19.66	10.47
Songgui	Barren	0.06	0.00	0.02	0.01	0	0	0	0	0.75	0.02	0.14	0.09	210.36	8.38	25.73	12.84

that the thermodynamic parameters can be applied to determine the chlorine melt content in equilibrium with apatite; the detailed function and results are given in the Online Material<sup>1</sup>. Using a set of natural and experimental apatite/melt partitioning data for andesitic to rhyolitic melts, Parat et al. (2011) calibrated the following empirical non-Henrian partitioning relationship for sulfur between apatite and melt:  $S_{\text{apatite}}(\text{wt}\%) = 0.0629 \times \ln S_{\text{melt}}(\text{wt}\%) + 0.4513$ .

The application of these calculations (Table 1) shows that fertile suites have higher Cl and S contents in the melt (Cl: 0–4.8 wt%; median 0.13 wt%, average 0.22 wt%; S: 8–3490 ppm; median 19 ppm, average 64 ppm), compared with barren suites (Cl: <0.33 wt%, median 0.001 wt%, average 0.01 wt%; S: <816 ppm, median 12 ppm, average 22 ppm). For example, the parental melt of the world-class Sarcheshmeh porphyry Cu deposit contained up to 3.8 wt% Cl and 14–28 ppm S. Comparative values are 0 to 3.2 wt% Cl and 10–395 ppm S in the Qulong porphyry Cu-Mo deposit, 0.03 to 0.9 wt% Cl and 9–86 ppm S in the Jiama porphyry-skarn Cu-Mo-Au deposit, and 0–4.8 wt% Cl and 15–827 ppm S in the Machangqing porphyry deposit (Table 1). These results are also similar with subduction-related porphyries system, the Corocochuayco Fe-Cu-Au porphyry-skarn deposit, Peru (Chelle-Michou and Chiaradia 2017), and Red Chris porphyry Cu-Au deposit in British Columbia (Zhu et al. 2018). This is consistent with other suggestions that high-Cl concentrations in the melts may be a prerequisite for the formation of porphyry-related ore deposits (Hsu et al. 2019). From fluid inclusion studies, the porphyry mineralization has shown that the hypersaline liquid and vapor are enriched in chlorine sulfur (Sillitoe 2010), which are consistent with the elevated chlorine and sulfur in magmatic apatite of fertile porphyries. It is commonly accepted that chlorine and sulfur are of paramount importance for supporting the transport and deposition of ore metals at magmatic-hydrothermal systems. Specifically, chlorine and sulfur are critical elements of ore-forming fluids due to their capacity to form ligands with ore metals such as Cu, Au, Pb, Zn, Fe, Mo, as well as, with other cations such as H<sup>+</sup>, K<sup>+</sup>, Na<sup>+</sup>, and Ca<sup>+</sup>, which permit their transport to the site of ore deposition and cause hydrothermal alteration (e.g., Chelle-Michou and Chiaradia 2017).

The <sup>87</sup>Sr/<sup>86</sup>Sr ratio in apatite can record the initial Sr isotopic

value of the magma, because Rb is highly incompatible in apatite ( $D_{\text{Rb}}^{\text{ap/melt}} = 0.0013$ ; Prowatke and Klemme 2006). The <sup>87</sup>Sr/<sup>86</sup>Sr ratios of apatites are similar in these whole-rock samples (e.g., Hou et al. 2015; Lu et al. 2015). The apatites in the fertile suites show a mantle <sup>87</sup>Sr/<sup>86</sup>Sr signature (0.704–0.706) and higher Cl/F, Cl, and S in the melts compared with barren plutons (Figs. 2d–2f), suggesting that the mantle source of the magmas also supplied the volatiles necessary for mineralization. The mantle origin of apatite in the fertile suites is further supported by apatite trace-element ratios (La/Sm and Th/U) consistent with previous findings of host-rock petrogenesis worldwide (Belousova et al. 2002; Figs. 2d and 2e).

### The recycled mantle origins of volatiles in the post-subduction porphyry deposits

The ore-forming magmas have higher Cl and S concentrations with less radiogenic <sup>87</sup>Sr/<sup>86</sup>Sr (Figs. 2e and 2f). We, therefore, use these Sr isotopes and Cl content modeled mixing between altered ocean crust (AOC; mean <sup>87</sup>Sr/<sup>86</sup>Sr 0.705; Sr 180 ppm; Staudigel et al. 1995; Cl 2000 ppm; Kendrick et al. 2017), post-subduction lithospheric mantle [PLM; Tibetan peridotite xenoliths with <sup>87</sup>Sr/<sup>86</sup>Sr, 0.714; Sr, 83.5 ppm (Xu et al. 2017); Cl: 200 ppm], and depleted MORB mantle (DMM; <sup>87</sup>Sr/<sup>86</sup>Sr, 0.7025; Sr, 15 ppm; Cl, 2 ppm (John et al. 2010)] to determine the sources of these volatiles. In this modeling, the chlorine from fertile porphyries requires almost 80% Cl contribution from AOC, with 10% post-subduction lithospheric mantle and/or 10% DMM (Fig. 2e). In contrast, apatite from barren suites inherits only 10–20% Cl from AOC (Fig. 2e). The plot of <sup>87</sup>Sr/<sup>86</sup>Sr vs. apatite S (Fig. 2f) also shows a large contribution from both AOC and DMM. This modeling suggests that the higher Cl and S contents of fertile porphyries are consistent with derivation primarily from dehydration of altered oceanic basalts during subduction. This is consistent with the high-chlorine concentration of serpentinized lithosphere (up to 2000 ppm Cl; Kendrick et al. 2017) and the positive δ<sup>34</sup>S compositions of arc magmas, consistent with those of seafloor sediments (de Hoog et al. 2001). Glass inclusions in olivine from primitive arc magmas have S concentrations up to 2900 ppm (de Hoog et al. 2001), and experimental A concentrations of oxidized arc basalts can be up to 1.5 wt% S (Jugo et al. 2005). These high-chlorine and high-

sulfur contents have significance for the behavior of chalcophile and siderophile metals in the genesis of porphyry Cu-Au deposit. The Cenozoic porphyry systems of Iran, Tibet, and western China developed in post-subduction settings when the AOC and DMM sources were no longer available. We thus propose that the higher chlorine and sulfur values in post-subduction Cu-Au deposits were derived from the SCLM metasomatized by previous oceanic subduction (Fig. 3).

In this model, the dehydration of altered oceanic slab (200–65 Ma; the period of during oceanic subduction) introduced a large amount of volatiles including Cl, S, and water into the SCLM of the mantle wedge (stage A; Fig. 3a), resulting in the formation of volatile-rich reservoirs in the SCLM. These may be documented by the presence of metasomatized phlogopite-bearing peridotite xenoliths entrained by Tibetan Miocene mantle-derived K-rich melts (phlogopite with 0.08 wt% Cl; Liu et al. 2011), hornblende- and phlogopite-bearing gabbro (Xu et al. 2019) in the Gangdese belts, and phlogopite- and apatite-bearing peridotites in NW Iran (Pang et al. 2013). During the continental collision that followed the subduction (stage B: ~15 Ma in Iran and Tibet; Fig. 3b), the existing volatile-bearing SCLM partially melted, with heat provided mainly by asthenospheric upwelling due to slab breakoff of the tearing or thinning of the passive continental lithospheric root (e.g., Xu et al. 2017), producing Cl- and S-enriched mantle-derived magmas (stage B; Fig. 3b). This generated widespread potassium-rich melts such as the Miocene Kerman, Miocene Gangdese, and Yunnan Eocene lamprophyres (Xu et al. 2017; Pang et al. 2013). These mafic melts underplated at the base of the crust, resulting in thermal and mass exchange during magma mixing and mingling with the overlying lower crust. This interaction led to the enrichment of volatiles in the lower crust, lowered melting temperatures to 700–750 °C (Lu et al. 2015) and promoted melting of mafic lower crust, and generated the shoshonitic and high-K calc-alkaline ore-forming porphyries (Yang et al. 2015).

The high-chlorine and high-sulfur contents of the magmas suppress the segregation of significant amounts of sulfide phases, leading to substantial metal enrichment in the evolving magma rather than in the cumulate rocks of the continental root. Thus, the degree of metal enrichment in the post-subduction settings, and the generation of world-class porphyry systems in such settings, depends on the availability of recycled chlorine and sulfur. Refertilization of the subcontinental lithospheric mantle by volatiles derived from earlier subduction is a key factor in forming post-subduction porphyries; this provides an alternative view to current ore enrichment models focusing on lower crust melting.

## IMPLICATIONS FOR EXPLORATION

### Porphyry systems

Relatively little geological work has been done in some areas of the Tethyan belt, such as Iran, Pakistan, Afghanistan, and even Tibet, and therefore the volatiles, trace-element contents, and Sr isotopes of apatite could usefully fingerprint fertile intrusions associated with mineralization. The robust trace-element ratios and Sr isotopes of apatite can record more information, especially of Cl and S evolution, which are key to the genesis of porphyry systems. Analyzing the compositions of apatite from an area with little geologic information or poor outcrop could efficiently and cheaply discriminate whether the drainage source area is domi-

nated by unlikely prospective crustally derived granitoids or by prospective mantle-associated granitoids. This could help to focus exploration on the most prospective areas.

Large porphyry ore deposits can be formed by combinations of “common” geological processes, but all of these processes must be optimized to form a giant deposit. The data presented here suggest that higher volatile contents are advantageous for forming large porphyry deposits because of the optimization of ore-metal transport in such chlorine- and sulfur-rich fluids

### Concluding remarks

Robust trace-element and Sr isotope data on apatite can distinguish fertile (porphyry Cu ± Au) magmas from barren magmatic suites. The fertility indicators are Cl/F (>0.19), V/Y (>0.008), and (Ce/Pb)<sub>N</sub> ratios (>2138), which are higher than in apatite from the barren suites; these elevated ratios reflect a volatile-enriched magma. Their less radiogenic Sr isotopes indicate that the higher volatile contents advantageous for ore-metal transport such chlorine- and sulfur-rich fluids reflect the derivation from the previously metasomatized mantle. This observation indicates the importance of volatiles, recycled from previous oceanic subduction, in collisional settings.

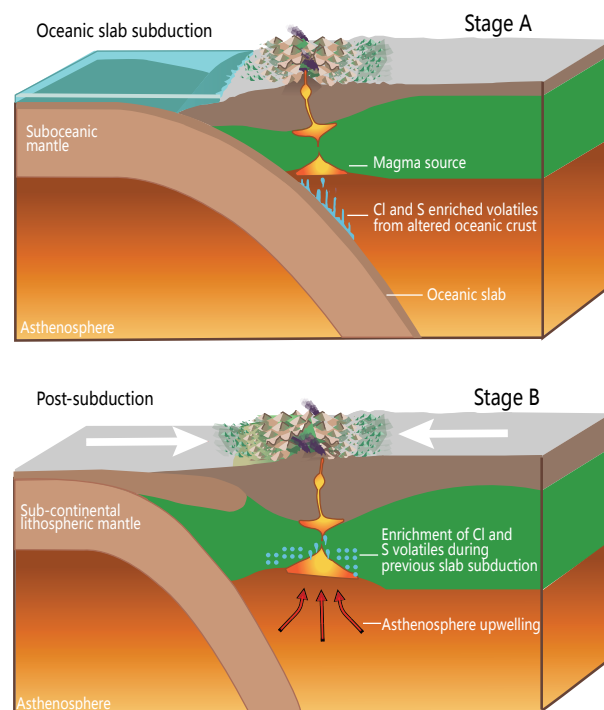


**FIGURE 3.** Evolution of volatiles in post-subduction setting. (a) Stage A: during oceanic slab subduction, dehydration of the subducting oceanic crust leads to partial melting of asthenosphere. Volatile-enriched basaltic melts intrude the overlying lithosphere and enrich Cl, S, and water at continental root, generate metasomatized phlogopite-bearing SCLM. (b) Stage B: during continental collision period, upwelling of asthenospheric mantle triggers remelting of previous metasomatized volatile-enriched SCLM, introduced melts capable of scavenging chlorine and sulfur from formerly enriched lithospheric root. Underplate of these Cl- and S-rich mafic magma mixing and mingling with the overlying lower crust, leading to formation of fertile magmas for post-collisional porphyry systems.

## ACKNOWLEDGMENTS AND FUNDING

This research was funded by National Key Technologies R&D Program 2019YFA0708602, 2016YFC0600310, National Natural Science Foundation of China (42073038, 41803045), Young Talent Support Project of CAST, Fundamental Research Funds for the Central Universities and IGCP-662. The analytical data were obtained using instrumentation funded by DEST Systemic Infrastructure Grants, ARC LIEF, NCRIS/AuScope, industry partners and Macquarie University. We thank the editor Hongwu Xu, associate editor Fang-Zhen Teng and constructive comments from two reviewers, which helped in improving our paper. This is contribution 1541 from the ARC Centre of Excellence for Core to Crust Fluid Systems (<http://www.ccfms.mq.edu.au>) and 1409 in the GEMOC Key Centre (<http://www.gemoc.mq.edu.au>).

## REFERENCES CITED

- Belousova, E.A., Griffin, W.L., O'Reilly, S.Y., and Fischer, N.I. (2002) Apatite as an indicator mineral for mineral exploration: Trace-element compositions and their relationship to host rock type. *Journal of Geochemical Exploration*, 76(1), 45–69.
- Brenan, J. (1993) Kinetics of fluorine, chlorine and hydroxyl exchange in fluorapatite. *Chemical Geology*, 110(1-3), 195–210.
- Brenan, J.M., Shaw, H.F., Ryerson, F.J., and Phinney, D.L. (1995) Mineral-aqueous fluid partitioning of trace elements at 900 °C and 2.0 GPa: Constraints on the trace element chemistry of mantle and deep crustal fluids. *Geochimica et Cosmochimica Acta*, 59(16), 3331–3350.
- Bruand, E., Storey, C., Fowler, M., and Heilimo, E. (2019) Oxygen isotopes in titanite and apatite, and their potential for crustal evolution research. *Geochimica et Cosmochimica Acta*, 255, 144–162.
- Chelle-Michou, C., and Chiaradia, M. (2017) Amphibole and apatite insights into the evolution and mass balance of Cl and S in magmas associated with porphyry copper deposits. *Contributions to Mineralogy and Petrology*, 172(11-12), 105.
- Chiaradia, M. (2014) Copper enrichment in arc magmas controlled by overriding plate thickness. *Nature Geoscience*, 7(1), 43.
- Davidson, J., Turner, S., Handley, H., Macpherson, C.G., and Dosseto, A. (2007) Amphibole “sponge” in arc crust? *Geology*, 35(9), 787–790.
- de Hoog, J.C.M., Mason, P.R.D., and van Bergen, M.J. (2001) Sulfur and chalcophile elements in subduction zones: Constraints from a laser ablation ICP-MS study of melt inclusions from Galunggung Volcano, Indonesia. *Geochimica et Cosmochimica Acta*, 65, 3147–3164.
- Ewart, A., and Griffin, W.L. (1994) Application of proton-microprobe data to trace-element partitioning in volcanic rocks. *Chemical Geology*, 117(1-4), 251–284.
- Griffin, W.L., Begg, G.C., and O'Reilly, S.Y. (2013) Continental-root control on the genesis of magmatic ore deposits. *Nature Geoscience*, 6(11), 905.
- Hou, Z., Yang, Z., Lu, Y., Kemp, A., Zheng, Y., Li, Q., and Duan, L. (2015) A genetic linkage between subduction- and collision-related porphyry Cu deposits in continental collision zones. *Geology*, 43(3), 247–250.
- Hsu, Y.-J., Zajacz, Z., Ulmer, P., and Heinrich, C.A. (2019) Chlorine partitioning between granitic melt and H<sub>2</sub>O-CO<sub>2</sub>-NaCl fluids in the Earth's upper crust and implications for magmatic-hydrothermal ore genesis. *Geochimica et Cosmochimica Acta*, 261, 171–190.
- Hughes, J.M., and Rakovan, J.F. (2015) Structurally robust, chemically diverse: Apatite and apatite supergroup minerals. *Elements*, 11(3), 165–170.
- John, T., Layne, G.D., Haase, K.M., and Barnes, J.D. (2010) Chlorine isotope evidence for crustal recycling into the Earth's mantle. *Earth and Planetary Science Letters*, 298(1-2), 175–182.
- Jugo, P.J., Luth, R.W., and Richards, J.P. (2005) Experimental data on the speciation of sulfur as a function of oxygen fugacity in basaltic melts. *Geochimica et Cosmochimica Acta*, 69(2), 497–503.
- Kendrick, M.A., Hémond, C., Kamenetsky, V.S., Danyushevsky, L., Devey, C.W., Rodemann, T., Jackson, M.G., and Perfit, M.R. (2017) Seawater cycled throughout Earth's mantle in partially serpentinized lithosphere. *Nature Geoscience*, 10(3), 222.
- La Tourrette, T.Z., Burnett, D.S., and Bacon, C.R. (1991) Uranium and minor-element partitioning in Fe-Ti oxides and zircon from partially melted granodiorite, Crater Lake, Oregon. *Geochimica et Cosmochimica Acta*, 55(2), 457–469.
- Li, H., and Hermann, J. (2017) The effect of fluorine and chlorine on trace element partitioning between apatite and sediment melt at subduction zone conditions. *Chemical Geology*, 473, 55–73.
- Liu, C.Z., Wu, F.Y., Chung, S.L., and Zhao, Z.D. (2011) Fragments of hot and metasomatized mantle lithosphere in Middle Miocene ultrapotassic lavas, southern Tibet. *Geology*, 39(10), 923–926.
- Loucks, R.R. (2014) Distinctive composition of copper-ore-forming arc magmas. *Australian Journal of Earth Sciences*, 61(1), 5–16.
- Lu, Y.J., Loucks, R.R., Fiorentini, M.L., Yang, Z.M., and Hou, Z.Q. (2015) Fluid flux melting generated post-collisional high-Sr/Y copper-ore-forming water-rich magmas in Tibet. *Geology*, 43, 583–586.
- Mao, M., Rukhlov, A.S., Rowins, S.M., Spence, J., and Coogan, L.A. (2016) Apatite trace element compositions: A robust new tool for mineral exploration. *Economic Geology*, 111(5), 1187–1222.
- Nandedkar, R.H., Hürlimann, N., Ulmer, P., and Müntener, O. (2016) Amphibole-melt trace element partitioning of fractionating calc-alkaline magmas in the lower crust: An experimental study. *Contributions to Mineralogy and Petrology*, 171(8-9), 71.
- O'Reilly, S.Y., and Griffin, W.L. (2000) Apatite in the mantle: implications for metasomatic processes and high heat production in Phanerozoic mantle. *Lithos*, 53(3-4), 217–232.
- Pang, K.N., Chung, S.L., Zarrinkoub, M.H., Lin, Y.C., Lee, H.Y., Lo, C.H., and Khatib, M.M. (2013) Iranian ultrapotassic volcanism at ~11 Ma signifies the initiation of post-collisional magmatism in the Arabia-Eurasia collision zone. *Terra Nova*, 25(5), 405–413.
- Parat, F., and Holtz, F. (2005) Sulfur partition coefficient between apatite and rhyolite: the role of bulk S content. *Contributions to Mineralogy and Petrology*, 150(6), 643–651.
- Parat, F., Holtz, F., and Klügel, A. (2011) S-rich apatite-hosted glass inclusions in xenoliths from La Palma: Constraints on the volatile partitioning in evolved alkaline magmas. *Contributions to Mineralogy and Petrology*, 162(3), 463–478.
- Piccoli, P.M., and Candela, P.A. (2002) Apatite in igneous systems. *Reviews in Mineralogy and Geochemistry*, 48(1), 255–292.
- Prowatke, S., and Klemme, S. (2006) Trace element partitioning between apatite and silicate melts. *Geochimica et Cosmochimica Acta*, 70(17), 4513–4527.
- Sha, L.K., and Chappell, B.W. (1999) Apatite chemical composition, determined by electron microprobe and laser-ablation inductively coupled plasma mass spectrometry, as a probe into granite petrogenesis. *Geochimica et Cosmochimica Acta*, 63(22), 3861–3881.
- Sillitoe, R.H. (2010) Porphyry copper systems. *Economic Geology*, 105, 3–41.
- Staudigel, H., Davies, G.R., Hart, S.R., Marchant, K.M., and Smith, B.M. (1995) Large scale isotopic Sr, Nd and O isotopic anatomy of altered oceanic crust: DSDP/ODP sites 417/418. *Earth and Planetary Science Letters*, 130(1-4), 169–185.
- Suzuki, K., Adachi, M., Yamamoto, K., and Nakai, Y. (1992) Intra-grain distribution of REE and crystallization sequence of accessory minerals in the Cretaceous Busetsu Granite at Okazaki, central Japan. *Geochemical Journal*, 26(6), 383–394.
- Tassara, S., González-Jiménez, J.M., Reich, M., Schilling, M.E., Morata, D., Begg, G., and Barra, F. (2017) Plume-subduction interaction forms large auriferous provinces. *Nature Communications*, 8(1), 843.
- Webster, J.D., Tappen, C.M., and Mandeville, C.W. (2009) Partitioning behavior of chlorine and fluorine in the system apatite-melt-fluid. II: Felsic silicate systems at 200 MPa. *Geochimica et Cosmochimica Acta*, 73(3), 559–581.
- Xu, B., Griffin, W.L., Xiong, Q., Hou, Z.Q., O'Reilly, S.Y., Guo, Z., and Zheng, Y.C. (2017) Ultrapotassic rocks and xenoliths from South Tibet: Contrasting styles of interaction between lithospheric mantle and asthenosphere during continental collision. *Geology*, 45(1), 51–54.
- Xu, W., Zhu, D.C., Wang, Q., Weinberg, R.F., Wang, R., Li, S.M., and Zhao, Z.D. (2019) Constructing the Early Mesozoic Gangdese crust in Southern Tibet by hornblende-dominated magmatic differentiation. *Journal of Petrology*, 60(3), 515–552.
- Yang, Z.M., Lu, Y.J., Hou, Z.Q., and Chang, Z.S. (2015) High-Mg diorite from Qulong in southern Tibet: Implications for the genesis of adakite-like intrusions and associated porphyry Cu deposits in collisional orogens. *Journal of Petrology*, 56(2), 227–254.
- Zhu, J.J., Richards, J.P., Rees, C., Creaser, R., and Jürgen Lang. (2018) Elevated magmatic sulfur and chlorine contents in ore-forming magmas at the red chris porphyry Cu-Au deposit, northern British Columbia, Canada. *Economic Geology*, 113, 1047–1075.

MANUSCRIPT RECEIVED JULY 12, 2020

MANUSCRIPT ACCEPTED OCTOBER 23, 2020

MANUSCRIPT HANDLED BY FANG-ZHEN TENG

## Endnote:

<sup>1</sup>Deposit item AM-21-47714, Online Material. Deposit items are free to all readers and found on the MSA website, via the specific issue's Table of Contents (go to [http://www.minsocam.org/MSA/AmMin/TOC/2021/Apr2021\\_data/Apr2021\\_data.html](http://www.minsocam.org/MSA/AmMin/TOC/2021/Apr2021_data/Apr2021_data.html)).